AN IMPULSE RADAR NONDESTRUCTIVE EVALUATION SYSTEM

Fu-Chiarng Chen and Weng Cho Chew
Electromagnetics Laboratory
Center for Computational Electromagnetics
Department of Electrical and Computer Engineering
University of Illinois, Urbana, IL 61801

INTRODUCTION

A microwave impulse radar system for nondestructive evaluation (NDE) and inverse scattering imaging has recently been developed at the University of Illinois [1,2]. This automated time-domain ultra-wideband radar system consists of a Picosecond Pulse Lab (PSPL) 4050B step generator, a PSPL 4050RPH remote pulse head, two PSPL 5210 impulse forming networks, a Hewlett-Packard (HP) 54120B digitizing oscilloscope mainframe, an HP 54121A 20 GHz four-channel test set, a broadband Vivaldi antenna [8] array, two ultra-wideband amplifiers and two microwave switches. The system is automated and controlled by a computer via the IEEE-488 bus. The performance of this impulse radar NDE system will be evaluated by collecting useful measurement data from different test targets including metallic and dielectric objects. Two iterative nonlinear image reconstruction algorithms, the distorted Born iterative method (DBIM) [3,4] and the local shape function (LSF) method [5,6,7], are used to process the time-domain measurement data to reconstruct the image of the target object. Our goal is to combine the impulse radar system and inverse scattering imaging algorithms to provide an NDE system with high resolution imaging capability for civil structures.

TIME-DOMAIN ULTRA-WIDEBAND RADAR SYSTEM

The time-domain impulse radar system has several advantages compared to the more conventional narrow-band CW radar system. For example, its ultra-wideband signal can provide much more information for target imaging and sensing. Also, it takes less measurement time and is less costly compared to the coherent step-frequency radar system.

The system block diagram of the time-domain impulse radar system is shown in Figure 1. The impulse radar system consists of a Hewlett-Packard (HP) 54120B digitizing oscilloscope mainframe, an HP 54121A 20 GHz four-channel test set, a

Picosecond Pulse Lab (PSPL) 4050B step generator, a PSPL 4050RPH remote pulse head, two PSPL 5210 impulse forming networks, a broadband Vivaldi antenna [8] array, two ultra-wideband amplifiers and two microwave switches. The one-dimensional ultra-wideband Vivaldi antenna array consists of 5 transmitting antennas and 6 receiving antennas. The Vivaldi antenna array is controlled by two microwave switches. To increase the system dynamic range, two ultra-wideband amplifiers are attached to the transmitting port and the receiving port. The radar system is automated and controlled by a computer via the IEEE-488 bus. The experimental arrangement of the Vivaldi antennas array and the object grid is shown in Figure 2. The distance between the transmitting antenna and receiving antenna is 8 cm. The distance of the object grid center to the antenna array is 40 cm.

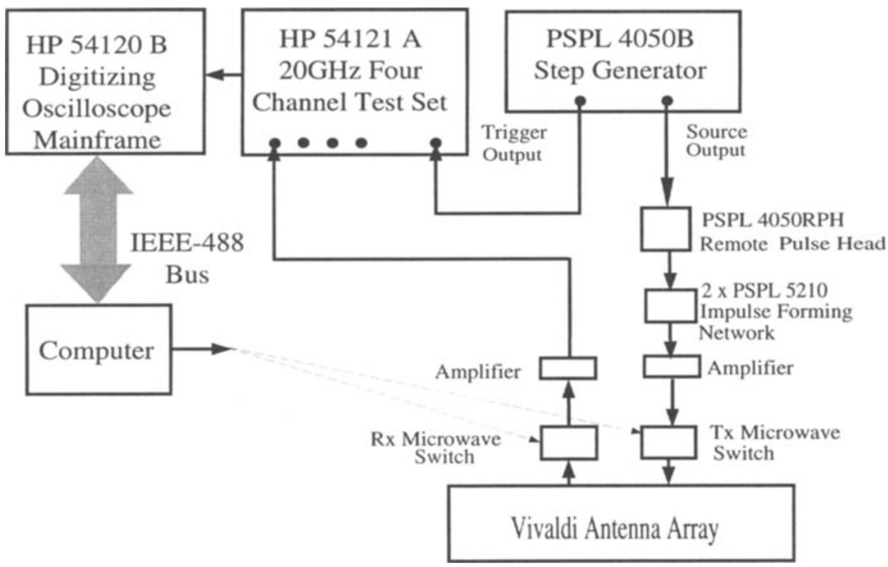

Figure 1. The time-domain pulse radar system.

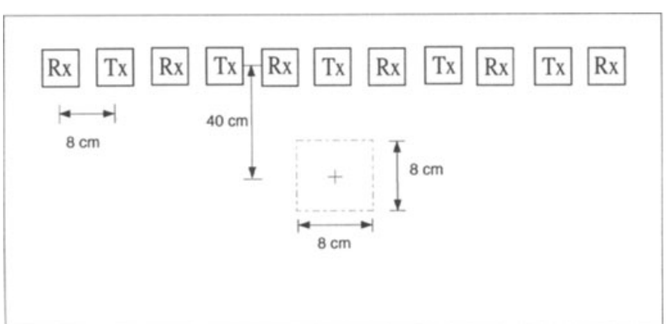

Figure 2. The experimental arrangement of the Vivaidi antenna array and the object grid. (Note: drawing not to scale.)

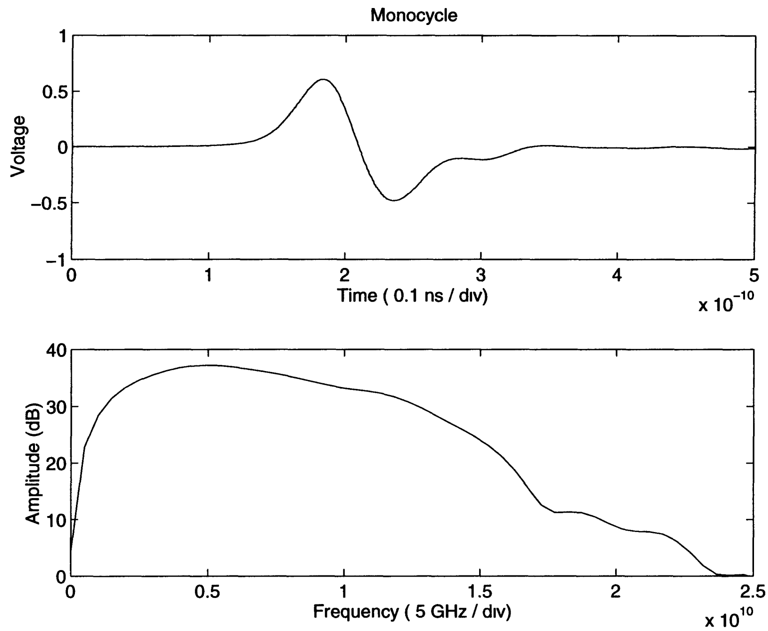

Figure 3. The time-domain profile and frequency spectrum of the monocycle pulse source.

A 10 volt, 45 ps rise-time pulse is generated by the PSPL 4050B step generator with the PSPL 4050RPH remote pulse head. A 2.5 volt, 50 ps impulse and a 1.5 V, 10 GHz monocycle pulse are generated by attaching 1 or 2 PSPL 5210 impulse forming networks to the output of the 4050RPH remote pulse head. The monocycle pulse is chosen as the transmitting signal to match the operational bandwidth of the Vivaldi antenna array. The time-domain plot and the frequency spectrum of the monocycle pulse are shown in Figure 3.

DATA ACQUISITOIN AND CALIBRATION

The evaluation of the impulse radar system has been done by collecting useful measurement data (30 sets) from the 5 transmitting and 6 receiving antennas in the Vivaldi antenna array. Figure 4 shows the 30 measurement data sets of the clutter (C) of the system without the test target. The clutter includes the background noise and the coupling between the transmitting antenna and receiving antenna. In Figure 4, we noticed the strong coupling effect between the transmitting antennas and receiving antennas of the Vivaldi antenna array around the time axis at 1 ns. Figure 5 shows the 30 measurement data sets of the metallic cylinder (M). In Figure 5, we can identify that small target signal is embedded in the time axis within a 3 ns to 4 ns range. Figure 6 shows the subtraction of the clutter data from the measurement data of the metallic cylinder. From Figure 5, we can clearly see the single reflected pulse signal from the metallic cylinder. However, this received reflected signal is not the actual value of the scattered field of the metallic cylinder. It is the value of the actual scattered field convolved with the system response (S) of the impulse radar system. Therefore, the effect of the system response must be removed out by a deconvolution process in order to obtain the actual scattered field value. This can be achieved by measuring a known reference target at a known position. The actual scattered field (T) of this reference target is known. The system response is equal to (R-C) deconvolved with T, where R is the measured reference target scattered field data, C is the measured clutter data and T is the actual scattered field of the reference target. After the system response value is obtained, the actual scattered field value of the metallic cylinder can be obtained by an additional deconvolution process to remove out the system response of the impulse radar system. The actual scattered field value of the metallic cylinder is equal to (M-C) deconvolved with S, where M is the measured metallic cylinder scattered field, C is the measured clutter data and S is the system response effect. The calibrated result is shown in Figure 7.

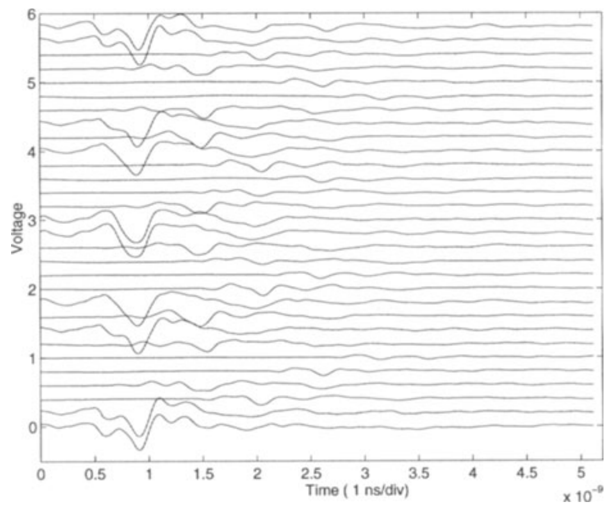

Figure 4. The measurement data (30 sets from the 5 transmitting antennas and 6 receiving antennas) of the clutter.

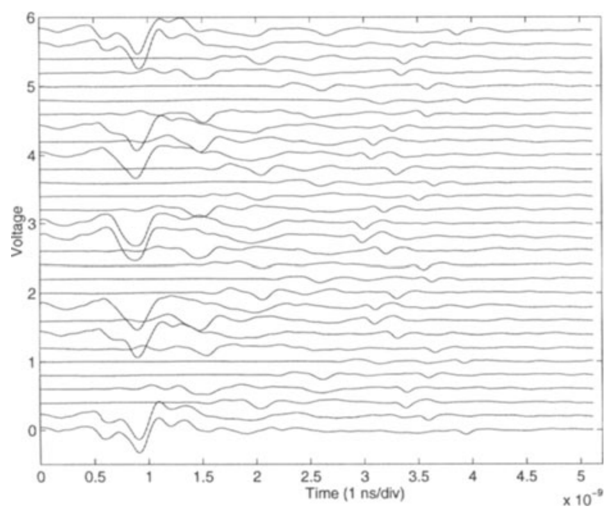

Figure 5. The measurement data (30 sets from the 5 transmitting antennas and 6 receiving antennas) of a metallic cylinder (3.2 cm in diameter).

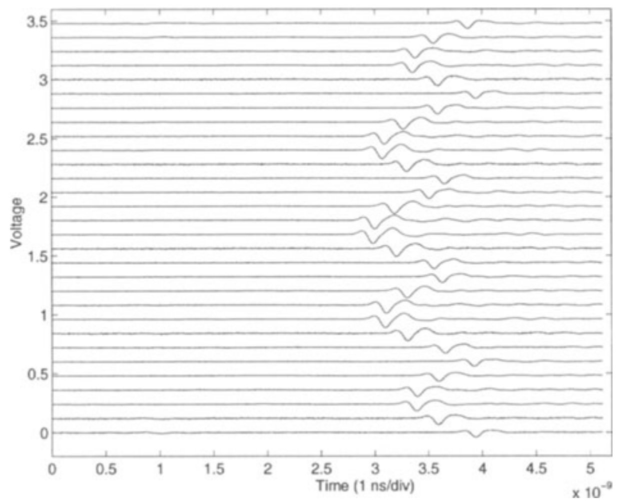

Figure 6. The subtraction of the clutter measurement data (Figure 3) from the metallic cylinder measurement data (Figure 4).

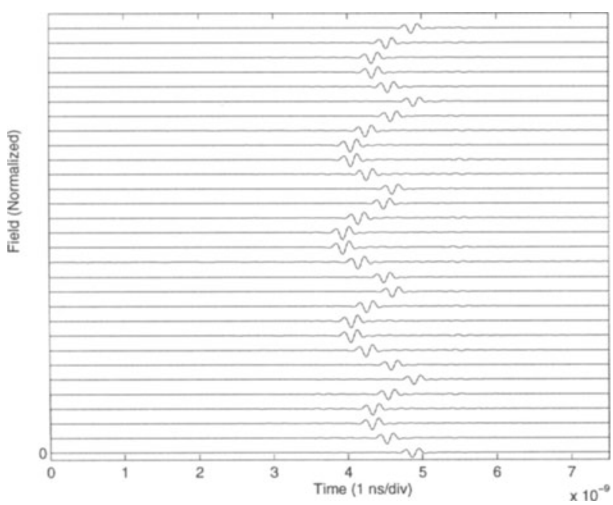

Figure 7. The calibrated normalized electrical field of the metallic cylinder.

INVERSE SCATTERING IMAGING

The calibrated 30 measurement data sets can be processed by inverse scattering imaging algorithms to obtain the reconstructed image of the test target. Two nonlinear iterative inverse scattering imaging algorithms, the Distorted Born Iterative Method (DBIM) [3,4] and the Local Shape Function (LSF) method [5,6,7] have been applied successfully to process the measurement data. Figure 8 shows the reconstructed permittivity image of a PVC pipe using the DBIM algorithm. The circular shape of the PVC pipe can be clearly observed and the reconstructed permittivity value of the PVC pipe is close to the actual value 2.5. Figure 9 shows the reconstructed image of a small metallic cylinder embedded in a concrete cement block using the LSF algorithm. The upper curvature is the shape of the concrete cement block. The lower part image is the image of the small metallic cylinder embedded 2 cm beneath the concrete cement block surface.

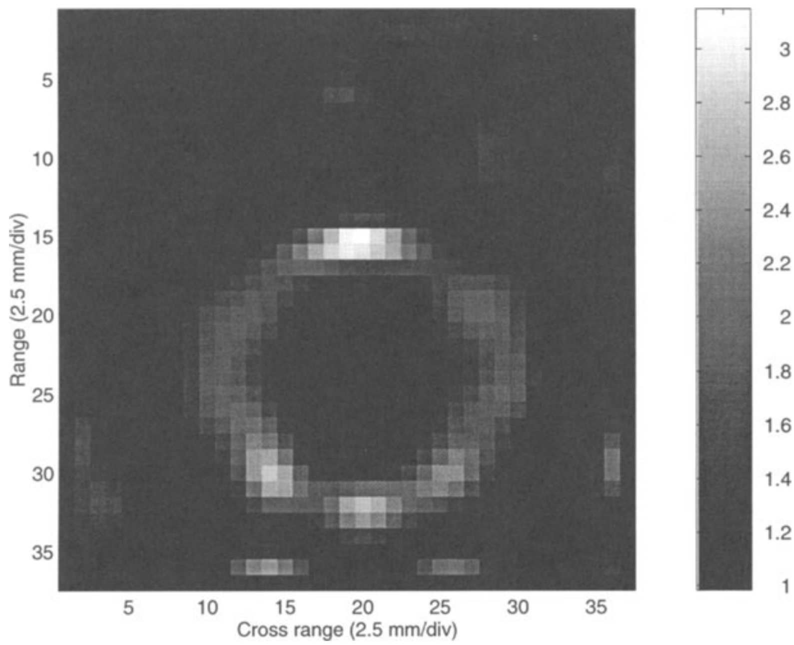

Figure 8. The DBIM reconstructed image of a plastic PVC pipe (4.8 cm in diameter).

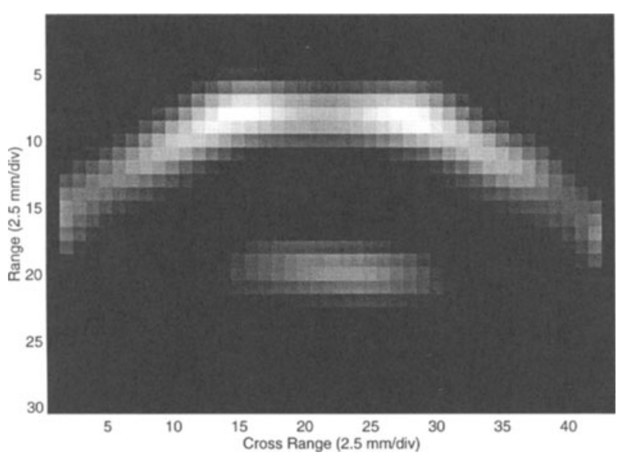

Figure 9. The LSF reconstructed image of a small metallic cylinder (1 cm in diameter) embedded 2 cm beneath a concrete cement block.

CONCLUSIONS

A new impulse radar system has been developed for nondestructive evaluation and inverse scattering imaging. The impulse radar system has been experimentally evaluated by collecting useful measurement data of different test targets. Two nonlinear iterative inverse scattering algorithms, the DBIM and the LSF, have been applied successfully to process the measurement data to obtain high resolution reconstruction images of the test targets. The results demonstrate that the combination of the impulse radar system and the inverse scattering imaging algorithms can provide a NDE system with a high resolution imaging capability for certain civil structures.

REFERENCES

1. F.-C. Chen and W. C. Chew, "Time-Domain Ultra-Wideband Radar System For Nondestructive Evaluation", *URSI Radio Science Meeting Digest*, Baltimore, Maryland, July 21-27, 1996.
2. F.-C. Chen, W. C. Chew, and W. H. Weedon, "Inverse Scattering Imaging Using Time-Domain Ultra-Wideband Radar", *URSI Radio Science Meeting Digest*, Baltimore, Maryland, July 21-27, 1996.
3. W. C. Chew, *Waves and Fields in Inhomogeneous Media.* New York: Van Nostrand, 1990.
4. W. C. Chew and Y. M. Wang, "Reconstruction of Two-Dimensional Permittivity Distribution Using the Distorted Born Iterative Method,", *IEEE Trans. Medical Imag.*, vol. 9, no. 2, pp. 218-225, 1990.
5. W. C. Chew and G. P. Otto,"Microwave Imaging of Multiple Metallic Cylinders Using Shape Functions," *Micro. Guided Wave Lett.*, vol. 2, no. 7, pp. 284-286, 1992.
6. G. P. Otto and W. C. Chew,"Microwave Inverse Scattering-Local Shape Function (LSF) Imaging for Improved Resolution of Strong Scatters,", *IEEE Trans. Microwave Theory Tech.*, Vol. MTT-42 No. 1, pp. 137-141, July 1994.
7. W. H. Weedon and W. C. Chew,"A Local Shape Function (LSF) Method for Time-Domain Inverse Scattering,", *IEEE Antennas and Propagation Society International Symposium Digest*, Ann Arbor, MI, June 28-July 2, 1993.
8. K. M. Frantz,"An Investigation of the Vivaldi Flared Radiator." M.S. thesis, University of Illinois at Urbana-Champaign, 1992.